Identifying Class Consensus and Differences in PPMI Parkinson's Dataset Using Node Ranking Approach

Kayle Boessen
i6075128

Course:	**MSB1014, Network Biology**
Program:	**Master Systems Biology and Bioinformatics**
Faculty:	**FSE**
Academic Year:	**2025/26**
Date:	**17/10/2025**

Maastricht University

1. Introduction

Parkinson's disease (PD) is a progressive neurodegenerative disorder affecting millions worldwide, characterized by motor and non-motor symptoms resulting from dopaminergic neuronal loss in the substantia nigra [1]. PD exhibits substantial clinical heterogeneity, patients present distinct symptom profiles, progression rates, and treatment responses [2]. Neuroimaging biomarkers have become essential for disease characterization and early detection, particularly dopamine transporter imaging, which reveals variable dopaminergic deficit patterns across patient populations [3].

Functional brain networks exhibit significant reorganization in PD, with alterations in both network structure and connectivity patterns detectable through resting-state functional MRI (rs-fMRI) [4]. Graph theory provides a quantitative framework for characterizing these network changes by representing brain regions as nodes and their functional connections as edges, enabling computation of topological metrics that capture network organization principles [5,6,7]. Recent investigations demonstrate that functional network disruptions relate to clinical manifestations including motor dysfunction and cognitive impairment, suggesting network topology can serve as a meaningful biomarker for disease phenotyping [8,9,10,11].

The heterogeneity of PD necessitates systematic approaches for identifying both consensus patterns shared across patient classes and distinctive features characterizing specific disease presentations. Node ranking and centrality-based analyses offer data-driven methods to prioritize brain regions based on their functional importance within network architectures [12,13].

The primary aim of this project is to identify nodes and edges that are either consistently present or reliably different across patient classes in a Parkinson’s dataset. The secondary aim is to produce a pipeline that generates reproducible networks and can be scaled for larger datasets.

2. Materials and Methods

Data. Correlation matrices of 20 subjects, precomputed by Xu, Yang [14], were selected to form the dataset. Each matrix represents pairwise correlations between 116 regions of interest (ROIs) in the brain, based on the automated anatomical labelling (AAL) atlas [15]. The correlation matrices are derived from rs-fMRI data captured by the Parkinson’s Progression Markers Initiative (PPMI). PPMI defines four classes of subjects: Parkinson’s (PD), Prodromal (PR), scans without evidence of dopaminergic deficit (SW), and healthy control (HC). The matrices were imported into R (version 4.4.2) using the *R.matlab* package [16].

Subject Network Construction. For each subject, an undirected functional network was inferred from the correlation matrix. To reduce noise and retain only the most meaningful connections, a threshold was introduced. A 95^{th} percentile cutoff was chosen to use as threshold. The correlations with values above the threshold were used to create an unweighted, undirected adjacency matrix. The resulting matrices were finally converted into graphs using the *igraph* package [17].

Class Consensus Network Construction. The subject networks were divided into classes based on their PPMI class. The networks within each class were combined into a consensus network to represent shared functional connectivity patterns. To construct these four networks, first an edge overlap matrix between the subject networks was computed. Then, pairwise Jaccard similarity was calculated between each subject pair and multiplied by a matrix of the shared edges between that pair, resulting in an edge weight matrix. These two matrices were summed, and finally, a weighted, undirected consensus graph was generated from the resulting adjacency matrix. Again, a 95th percentile threshold was applied to the (normalized) combined edge weight distribution to select the edges for the consensus network.

Node Ranking Analysis. The nodes of each consensus network were ranked on a scale of 1-116, based on four centrality measures: degree, betweenness, closeness, and Katz [18]. These centralities were computed using the packages *dplyr* [19] and *manynet* [20]. The four centrality ranks are averaged for each node, and then used to create an aggregate rank, also on a scale of 1-116 (in all rankings, an average method is used to resolve ties). Nodes with a degree of 0 were given an aggregate rank of 117 to show that they are disconnected from the network.

Network Similarity. Paired Jaccard similarity and Spearman rank correlation coefficients were calculated to quantify network similarity in terms of nodes and edges respectively. The consensus network of each patient class (PD, PR, and SW) was then merged with the HC network and given an edge weight: 2 for edges appearing in both networks, 1 for edges appearing in either. The nodes in these merged networks were classified by their rank difference, i.e. how much higher or lower the aggregate rank of a node in the patient class network is, compared to healthy control.

3. Results

The four class consensus networks (Figure 1A) display different functional connectivity patterns. The PD network has 353 edges, PR has 356 edges, SW has 340 edges and HC has 348 edges. The central nodes in the networks of the patient classes (PD, PR, and SW) rank higher compared to the healthy controls (HC).

The pairwise Jaccard similarity scores (Figure 2A) between the consensus networks indicate moderate similarity between all networks, where PD and PR are the most similar, HC and SW are the least similar. PD and PR have a slightly higher similarity with HC. This similarity distribution can also be seen when comparing the number of edges in the merged consensus networks (Figure 1B). More than half of PD edges overlap with HC, 65.2% (230 edges), for PR this is 65,7% (234 edges), and for SW 62,1% (211 edges). These overlapping edges with the three patient classes account for 66,1% of the original edges in the HC network with PD, 67,2% with PR, and 60,6% with SW. The aggregate rank difference as mapped in the merged networks shows an increase in rank for central nodes and a decrease in rank for more laterally spaced nodes when comparing patient to healthy control.

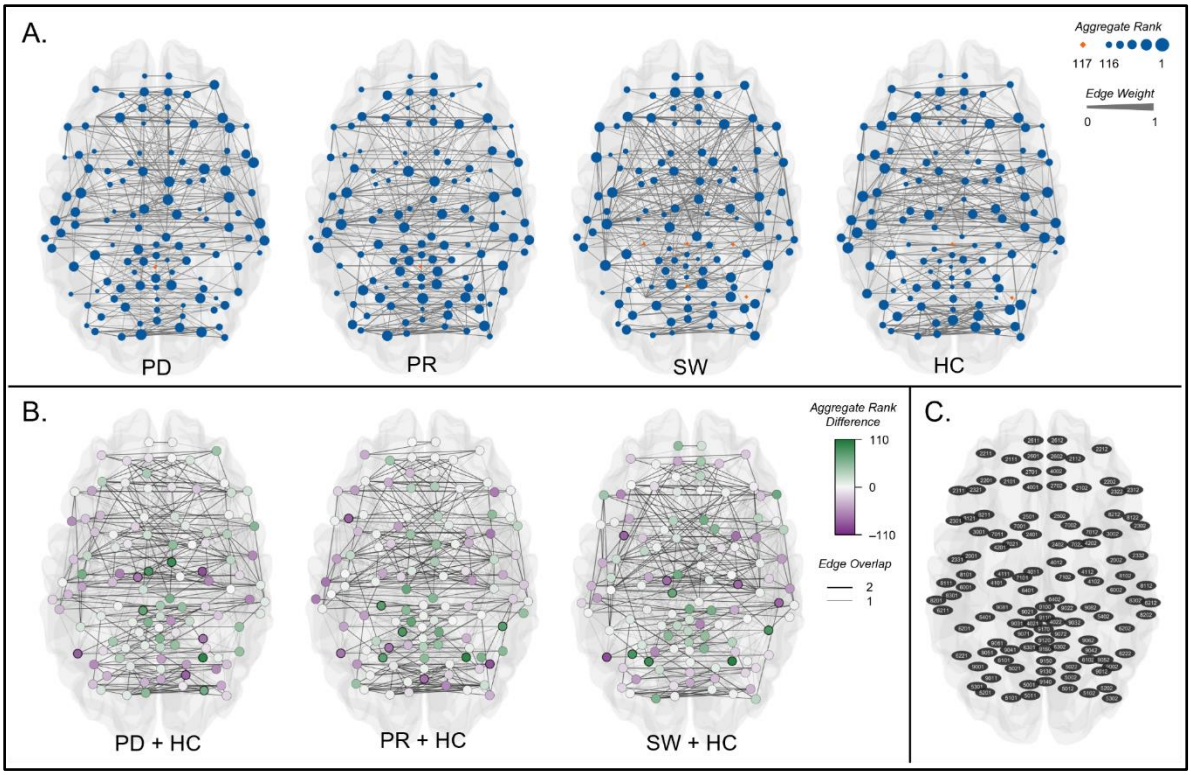

Figure 1. Consensus Networks

(A) *Four class consensus networks: PD, PR, SW, and HC. Node size indicates aggregate rank, shown as blue circles. Disconnected nodes (ranked 117) are shown as orange diamonds. Normalized, combined edge weight is shown as edge width.* ***(B)*** *Three merged consensus networks, merging each patient class with HC. The difference in aggregate rank of each node is indicated by a gradient (green: higher in patient class, purple: lower in patient class). The 10 most differential nodes (5 increased, 5 decreased) are circled in black. Edge overlap is shown in edge width and transparency (only the edges with value 2 are counted as part of the merged network).* ***(C)*** *Mapping of the network nodes to AAL atlas[15] ID numbers corresponding to brain ROIs.*

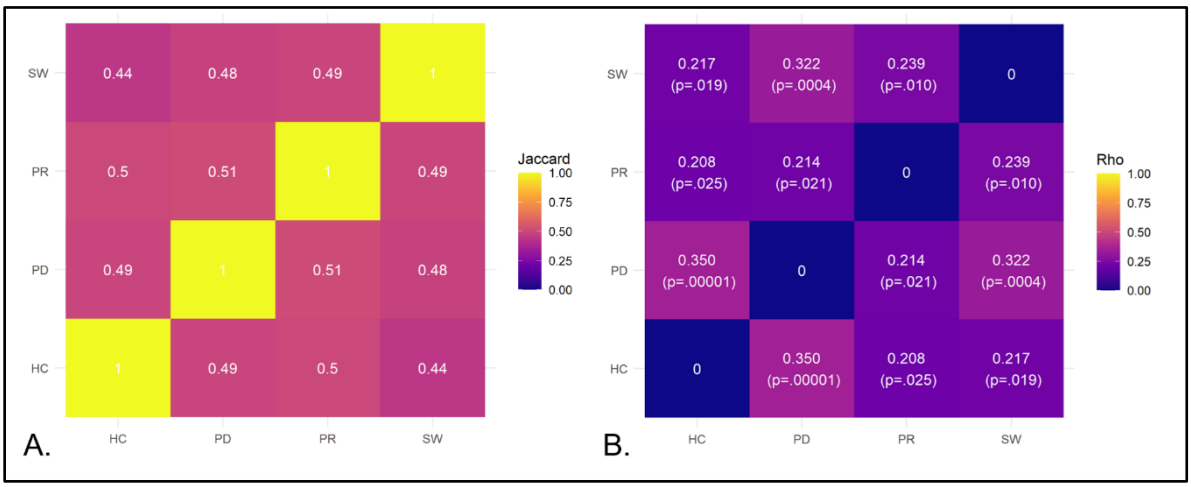

Figure 2. Consensus Network Similarity

These heatmaps show ***(A)*** *the pairwise Jaccard similarity scores and* ***(B)*** *the pairwise Spearman rank correlation test scores between the consensus networks of the four subject classes.*

In the scatterplots (Figure 3) of the aggregate rank differences in the merged networks, the nodes do not align on the diagonal for any of the three patient classes. Nodes above the diagonal indicate decreased rank in the patient class, while nodes in the bottom indicate increased rank. The spread of these rank differences shows once again the incongruency in both number and pattern of functional connections through nodes when comparing the patient classes to healthy controls. The node ranks of PD seem to differ more from those of HC than the node ranks of PR. This is consistent with the results of the Spearman rank correlation test (Figure 2B).

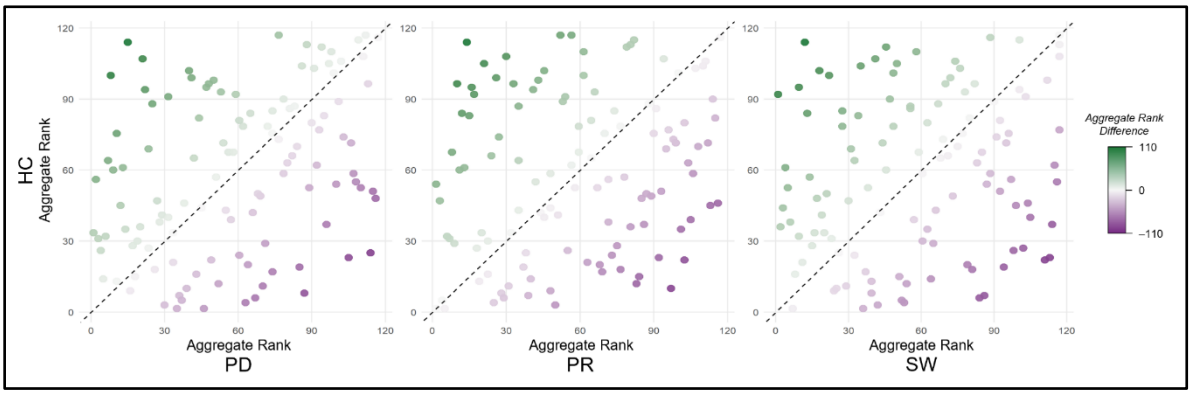

Figure 3. Aggregate Rank Difference Scatterplot

This scatterplot shows the aggregate rank of each node in the HC consensus network on the y axis and the ranks of the patient class nodes on the x axes. Green points indicate an increased aggregate rank in the patient classes compared to HC, purple points indicate a decreased aggregate rank.

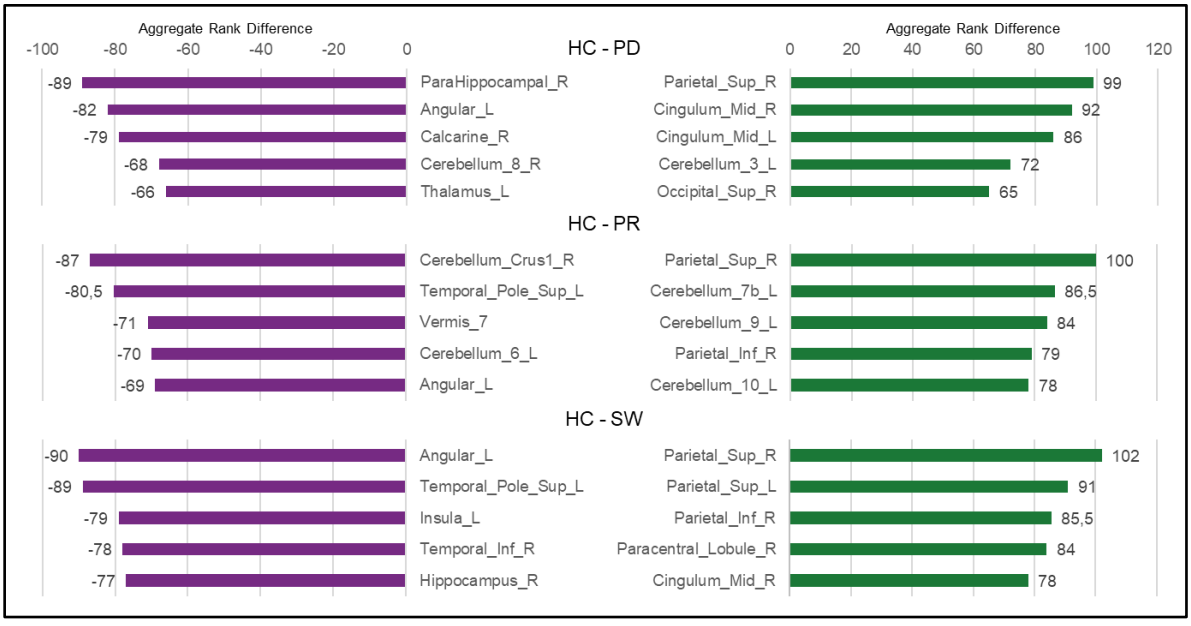

Figure 4. Most Differentially Ranked Nodes

This figure shows the 5 most differentially ranked nodes between the patient consensus network and healthy control. On the left side the 5 nodes that have the highest decrease in ranking compared to control, on the right side the 5 nodes with the highest increase in ranking compared to control. The nodes are labelled by the AAL atlas[15] name corresponding to the mapped atlas IDs (Figure 1C).

Ten nodes were selected from each merged network, the 5 nodes with the highest positive difference in aggregate node rank in the patient class compared to healthy control, and the 5 nodes with the highest negative difference in aggregate node rank. The selected nodes and their aggregate note rank difference can be seen in Figure 4. Across all patient classes, a strong increase in the rank of the nodes representing superior parietal and midcingulate regions is seen. The left angular gyrus node has a noticeably lower rank across all patient classes, and additional lower ranks are observed in nodes representing temporal pole (PR, SW) and thalamic/hippocampal regions (PD, SW).

4. Discussion

The aim of this research project was to find network differences between patient classes in the PPMI dataset, while building a reproducible workflow for bigger datasets. The preliminary results show significant difference in the importance of nodes in class consensus networks according to the Spearman rank correlation coefficient. Edge differences were confirmed using Jaccard similarity. Finally, differential node ranking across the patient classes revealed distinct topological changes that could reflect disease pathology and progression.

The consistent rank increase of superior parietal regions across all classes may be explained by compensation for visuospatial integration and postural control, consistent with reports of altered parietal connectivity in PD motor subtypes [4,21]. The pronounced decrease in angular gyrus rank could indicate disrupted default mode network function, aligning with documented DMN alterations in early-stage and manifested PD [22,23]. Class-specific patterns emerged too, with PR patients showing increased medial cerebellar connectivity, potentially reflecting motor prediction mechanisms before striatal degeneration becomes complete [24]. PD demonstrated a decrease in thalamus node rank, while in PR this node ranked higher (aggregate difference of -15), this could indicate progressive network disintegration. The decrease of temporal pole node rank in PR and SW suggests pre-dopaminergic limbic-temporal vulnerability, distinguishing early pathology from overt motor symptoms [23,25]. Decreased connectivity of the middle cingulum could indicate compensatory activation for cognitive control, or reflect altered integration of emotional and motor information processing [21,26].

A small dataset was used intentionally to be able to create a pipeline that can eventually handle larger datasets and can be tuned using different thresholding methods. These methods reduce noise but can also influence the results, which means that each dataset has to be analyzed first to decide on a cutoff value. The methodology further requires precomputed correlation matrices using AAL parcellated rs-fMRI data, which is quite specific. This was chosen because time constraints limited the amount of work that could be done and precomputed networks were a good starting point.

Overall, the pilot project produces possible evidence for functional reorganization in patient functional networks: SW shows pre-dopaminergic disruption, PR shows compensatory emergence, and PD indicates full network reorganization with loss of subcortical connectivity. When validated with larger datasets, this topology-based approach could improve early diagnostic specificity and stratify disease subtypes beyond traditional motor phenotyping.

5. Resources

Code, data, and results from this project, as well as high resolution version of the figures are available in the project GitHub repository: https://github.com/KBoessen/MSB1014-PPMI-Consensus-Project.git

Bibliography

1. Zhou ZD, Yi LX, Wang DQ, Lim TM, Tan EK. Role of dopamine in the pathophysiology of Parkinson's disease. Translational Neurodegeneration. 2023;12(1):44.
2. Markello RD, Shafiei G, Tremblay C, Postuma RB, Dagher A, Misic B. Multimodal phenotypic axes of Parkinson's disease. npj Parkinson's Disease. 2021;7(1):6.
3. Erro R, Schneider SA, Stamelou M, Quinn NP, Bhatia KP. What do patients with scans without evidence of dopaminergic deficit (SWEDD) have? New evidence and continuing controversies. J Neurol Neurosurg Psychiatry. 2016;87(3):319-23.
4. Chen X, Liu M, Wu Z, Cheng H. Topological Abnormalities of Functional Brain Network in Early-Stage Parkinson's Disease Patients With Mild Cognitive Impairment. Frontiers in Neuroscience. 2020;Volume 14 - 2020.
5. Zhang J, Wang H, Zhao Y, Guo L, Du L, Alzheimer's Disease Neuroimaging I. Identification of multimodal brain imaging association via a parameter decomposition based sparse multi-view canonical correlation analysis method. BMC bioinformatics. 2022;23(Suppl 3):128.
6. Bergamino M, Keeling EG, Ray NJ, Macerollo A, Silverdale M, Stokes AM. Structural connectivity and brain network analyses in Parkinson's disease: A cross-sectional and longitudinal study. Frontiers in Neurology. 2023;Volume 14 - 2023.
7. Ryyppö E, Glerean E, Brattico E, Saramäki J, Korhonen O. Regions of Interest as nodes of dynamic functional brain networks. Netw Neurosci. 2018;2(4):513-35.
8. Rucco R, Lardone A, Liparoti M, Lopez ET, De Micco R, Tessitore A, et al. Brain networks and cognitive impairment in Parkinson's disease. bioRxiv. 2020:2020.12.14.422706.
9. Kinugawa K, Mano T, Sugie K. Changes in brain functional connectivity between on and off states and their relationship with cognitive impairment in Parkinson's disease. Scientific Reports. 2024;14(1):27333.
10. Maiti B, Rawson KS, Tanenbaum AB, Koller JM, Snyder AZ, Campbell MC, et al. Functional Connectivity of Vermis Correlates with Future Gait Impairments in Parkinson's Disease. Movement Disorders. 2021;36(11):2559-68.
11. Liu Q, Shi Z, Wang K, Liu T, Funahashi S, Wu J, et al. Treatment Enhances Betweenness Centrality of Fronto-Parietal Network in Parkinson's Patients. Front Comput Neurosci. 2022;16:891384.
12. Ryan B, Marioni RE, Simpson TI. An Integrative Network Approach for Longitudinal Stratification in Parkinson's Disease. medRxiv. 2024:2024.01.25.24301595.
13. Herrington TM, Briscoe J, Eskandar E. Structural and Functional Network Dysfunction in Parkinson Disease. Radiology. 2017;285(3):725-7.
14. Xu J, Yang Y, Huang DTJ, Gururajapathy SS, Ke Y, Qiao M, et al. Data-Driven Network Neuroscience: On Data Collection and Benchmark. 2023.
15. Tzourio-Mazoyer N, Landeau B, Papathanassiou D, Crivello F, Etard O, Delcroix N, et al. Automated Anatomical Labeling of Activations in SPM Using a Macroscopic Anatomical Parcellation of the MNI MRI Single-Subject Brain. NeuroImage. 2002;15(1):273-89.
16. Bengtsson H, Jacobson A, Riedy J. R.matlab: Read and Write MAT Files and Call MATLAB from Within R. Version 3.7.0 ed2022.
17. Csárdi G, Nepusz T. The igraph software package for complex network research. 2.1.4 ed: InterJournal; 2006.
18. Katz L. A new status index derived from sociometric analysis. Psychometrika. 1953;18(1):39-43.
19. Wickham H, François R, Henry L, Müller K, Vaughan D. dplyr: A Grammar of Data Manipulation. R package version 1.1.4 ed2025.
20. Hollway J, Sposito H, Steglich C. manynet: Many Ways to Make, Modify, Mark, and Measure Myriad Networks. Version 1.6.1 ed2025.
21. Tinaz S. Functional Connectome in Parkinson's Disease and Parkinsonism. Current Neurology and Neuroscience Reports. 2021;21(6):24.

22. Zhou F, Tan C, Song C, Wang M, Yuan J, Liu Y, et al. Abnormal intra- and inter-network functional connectivity of brain networks in early-onset Parkinson’s disease and late-onset Parkinson’s disease. Frontiers in Aging Neuroscience. 2023;Volume 15 - 2023.
23. Wei J, Lyu J, Xiang J, Niu Y, Yang L, Fan C, et al. Impaired Brain Information Transmission Efficiency and Flexibility in Parkinson’s Disease and Rapid Eye Movement Sleep Behavior Disorder: Evidence from Functional Connectivity and Functional Dynamics. Parkinson's Disease. 2022;2022(1):7495371.
24. Gardoni A, Agosta F, Sarasso E, Basaia S, Canu E, Leocadi M, et al. Cerebellar alterations in Parkinson’s disease with postural instability and gait disorders. Journal of Neurology. 2023;270(3):1735-44.
25. Shang S, Zhu S, Wu J, Xu Y, Chen L, Dou W, et al. Topological disruption of high-order functional networks in cognitively preserved Parkinson's disease. CNS Neurosci Ther. 2023;29(2):566-76.
26. Sarasso E, Gardoni A, Zenere L, Emedoli D, Balestrino R, Grassi A, et al. Neural correlates of bradykinesia in Parkinson's disease: a kinematic and functional MRI study. NPJ Parkinsons Dis. 2024;10(1):167.